Optimization of Coal Particle Flow Patterns in Low NO_x Burners

Technical Progress Report

Due October 29, 1999

Prepared by

Jost O.L. Wendt and Gregory E. Ogden
Dept. of Chemical & Environmental Engineering
University of Arizona
Tucson, AZ 85721

Jennifer Sinclair and Caner Yurteri
School of Chemical Engineering
Purdue University
West Lafayette, IN 47907

Submitted to

DOCUMENT CONTROL CENTER,
U.S. Department of Energy
University Coal Research Program
Pittsburgh Energy Research Center
P.O. Box 10940, MS 921-0940
Pittsburgh, PA 15236-0940.

Under Contract DE-FG26-97FT97269

August 20, 2001

INTRODUCTION

The proposed research is directed at evaluating the effect of flame aerodynamics on NO_x emissions from coal fired burners in a systematic manner. This fundamental research includes both experimental and modeling efforts being performed at the University of Arizona in collaboration with Purdue University. The objective of this effort is to develop rational design tools for optimizing low NO_x burners to the kinetic emissions limit (below 0.2 lb./MMBTU). Experimental studies include both cold and hot flow evaluations of the following parameters: flame holder geometry, secondary air swirl, primary and secondary inlet air velocity, coal concentration in the primary air and coal particle size distribution. Hot flow experiments will also evaluate the effect of wall temperature on burner performance.

Cold flow studies will be conducted with surrogate particles as well as pulverized coal. The cold flow furnace will be similar in size and geometry to the hot-flow furnace but will be designed to use a laser Doppler velocimeter/phase Doppler particle size analyzer. The results of these studies will be used to predict particle trajectories in the hot-flow furnace as well as to estimate the effect of flame holder geometry on furnace flow field. The hot-flow experiments will be conducted in a novel near-flame down-flow pulverized coal furnace. The furnace will be equipped with externally heated walls. Both reactors will be sized to minimize wall effects on particle flow fields.

The cold-flow results will be compared with Fluent computation fluid dynamics model predictions and correlated with the hot-flow results with the overall goal of providing insight for novel low NO_x burner geometry's.

CURRENT PROGRESS

The bulk of the research efforts during this time period were conducted at Purdue with the Cold-Flow furnace.

Cold-Flow Studies-Purdue University

The two-phase system utilized for this study is an axisymmetric particle-laden coaxial jet. The spherical glass beads particles used in the experiments have a nominal diameter of 70 microns with 80% between 63 to 85 microns. Glass beads with a nominal diameter of 4-5 microns are used as the seed particles for the LDV measurements of the gas phase. The specific gravity of both particles and seeds is 2.5. The schematic of the coaxial jet flow apparatus is shown in Figure 1. The airflow to the central nozzle is mixed with the particles stored in the hopper through a venturi-type inductor and with the seed through a reverse cyclone. The central nozzle is a 14.22 mm (0.56 inch) ID copper pipe with a wall thickness of 1.65 mm (0.65 inch). The length to diameter ratio for the central nozzle is 100 to ensure a fully developed, turbulent pipe flow at the pipe exit. The flow to the annular nozzle is mixed with the seed particles before it is discharge to the 0.46 x 0.46 m (18x18 inches) chamber. The inner diameter ratio between the annular and the central nozzle is 2.24. Flow straighteners in the form of perforated plates are inserted in order to eliminate any swirl in the annular section. Figure 2 displays a detailed schematic of the central and annular section.

The particles are collected at the bottom of the chamber and weighed with a load cell so that the mass flow rate of particles can be monitored.

Laser Doppler Velocimetry / Phase Doppler Particle Analyzer (LDV/PDPA)

A two-component laser Doppler velocimetry / phase Doppler particle analyzer (LDV/PDPA) was used to make measurements of the mean and fluctuating velocity of particles, as well as the particle size. The LDV/PDPA system is placed on a X-Y-Z traversing system with a 10^{-4} inch accuracy. A 5-W argon ion laser, with blue and green beam wavelengths of 488 and 514 nm, respectively, is used as the light source. The system uses a Bragg cell unit that created a 40 MHz frequency shift for one of each of the color beams to avoid directional ambiguity. The size of the optical measurement volume is 100 x 233 x 233 μm.

For the single-phase measurements, the high voltage of the photomultiplier tube (PMTs) was set at 350 V and the burst threshold was set at 0.05 mV for the seed particles. To measure the 70 μm particles in two-phase flow, the PMTs were set at 250 V with a burst threshold of 1 mV. A minimum of 1,000 coincident samples is collected for both phases to minimize the statistical error. The coincidence mode is employed in order to ensure that both the burst signal from the green and blue beams originate from the same particle. Hardalupas *et al.* stated that the random errors for the mean axial velocity, the axial and radial fluctuating velocities are 1%, 3%, and 5%, respectively (1). The manufacturer of the LDV/PDPA system reported that the random error in the particle size measurement is 1%.

Experimental Flow Conditions

The central jet was loaded with spherical glass beads at a mass loading, m of 0.5. The solid loading m is defined as the mass flow rate ratio of particles to air. Three velocity ratios of 0, 1, and 1.8 were undertaken to investigate the effect of the annular jet on the particle motion. The Reynolds number for the central jet at the nozzle exit was maintained constant at 8,300 and the annular flow velocity was varied. Table 1 lists the experimental conditions for the single-phase and two-phase flows.

Experimental Results and Discussions
Particle Stokes number (St)

Table 2 lists the particle St for different axial positions for the three velocity ratios. For simplicity, the fluid time scale, τ_f, is calculated based on the mean flow properties. The length scale of the fluid is taken as the half-jet width, and the velocity scale of the fluid is the centerline axial mean gas velocity.

It is important to evaluate the particle St in order to investigate the effect of the gas turbulence on the particle fluctuation velocities and the particle radial motion. The particle St at the nozzle exit is greater than 10, indicating that the particle is unresponsive to gas turbulence. By the axial location, $x/d_i = 10$, the St is on the order of ten, still corresponding to unresponsive particles. Based on this value of the particle St, the particle motion in the measurement distance will not be affected by the turbulent eddies.

Nozzle Exit Measurements

The nozzle exit measurements were taken at distance of 1 mm downstream of the nozzle exit. Figure 3a displays the radial profiles of the axial mean gas velocity, U_g and the axial mean particle velocity, U_p at the nozzle exit. The profile of the axial mean gas velocity represents the 1/7 power law profile of turbulent pipe flow. The axial mean particle velocity has a flat profile across the pipe diameter with particle slip condition on the pipe wall. The particles in the pipe interact with the gas through a drag force, causing the presence of a slip velocity, $Us = U_g - U_p$. The mean slip velocity is 2.8 m/s in the pipe centerline and - 8.5 m/s on the pipe wall.

The radial motions of particles and gas at the nozzle exit are displayed in Figure 3b. The radial mean particle velocity, V_p is about zero across the central jet diameter, but it increases significantly near the wall. This may be due to the interaction between the particles and turbulent eddies and due to the lift force in the wall boundary layer. It is interesting to note that particles move radially with a higher radial velocity than that of the gas even though the particle St is higher than 10.

The radial variations in the axial and radial fluctuating velocities for both gas and particles are displayed in Figures 3c and 3d, respectively. The particles have higher axial and radial fluctuating velocities than those of the gas near the pipe centerline. This behavior has been observed previously (1). This may be due to the particle-particle collisions in the pipe centerline because the particle volume fraction has a normal distribution in the fully developed pipe.

Axial Mean Gas and Particle Velocity

Figures 4a and 4b show the experimental data of the axial mean velocities for both gas and particles at axial locations, x/d_i, of 3 and of 10, respectively. Comparing the profiles of the axial mean gas velocity for different velocity ratios, it increases with an increase in the velocity ratio. When the velocity ratio is 1 or larger, the annular jet fluid will move inward and transfer its mass and its momentum to the central jet fluid through the inner shear layer. The higher the velocity ratio, the more momentum will be transferred to the central jet. The mixing process will increase the volumetric flow rate in the region where particles are present and will influence the volume fraction profile.

Due to the change in the gas velocity, the gas-solid interactions will also change. As the velocity ratio increases, the gas will accelerate the particle axial mean velocity with a higher drag force. The gas will stop accelerating the particles when both the magnitudes of the axial mean gas velocity and the axial mean particle velocity are the same. Then, as the particle moves faster than the gas as shown by the case with velocity ratio of 0 at x/d_i of 10, the particle will accelerate the gas.

The increase in the velocity ratio will influence two things that are important for NO_x emissions. First, the velocity ration increase will increase the partial pressure of oxygen in the fluid surrounding the particles, which increases the stochiometric ratio as the

particle mass flow rate is the same for all velocity ratios, assuming no particle loss. Second, the increase in the velocity ratio will increase particle axial mean velocity, therefore decreasing particle residence time in the devolatilization region.

Radial Mean Gas and Particle Velocity

Figure 5 displays the radial mean particle velocity, V_p at x/d_i of 3 and 10 and Figure 6 displays the radial mean gas velocity, V_g. The radial profile of the radial mean gas velocity increases with radial distance. The radial mean gas velocity for the case with velocity ratio of 0 is higher near the jet centerline at x/d_i of 3 than the other cases since it has a narrower jet width. By x/d_i of 10, the radial mean gas velocity increases with an increase in the velocity ratio. The radial mean particle velocity is an important parameter because it determines the radial dispersion of the particles, changing the particle concentration distribution across the flow. The radial mean particle velocity is about the same for all velocity ratios at x/d_i of 3, but at x/d_i of 10, the radial mean particle velocity is higher for the case with a higher velocity ratio.

It is a question of interest to answer how the radial mean particle velocity changes with the velocity ratio. The effect of gas turbulence should be minimum since the particle St is on the order of ten for the axial distances observed. Figure 7 shows that the axial evolution of the axial fluctuating gas and particle velocity along the jet centerline between the inlet and $x/d_i = 10$. There is no change in the axial particle fluctuating velocity although the particles are exposed to higher turbulence for the higher velocity ratio case. This verifies that gas turbulence does not affect the particle motion, as predicted by the particle Stokes number. Therefore, the only source for the observed behavior in the radial mean particle velocity is the interaction between the particles and the mean gas radial velocity. Comparing Figures 5 and 6, the radial mean velocity of the particles is higher than that of the gas. Consequently, the gas will reduce the radial mean particle velocity via a drag force.

There are two reasons for the observed trend in the radial mean particle velocity at $x/d_i = 10$. First, the radial mean gas velocity increases with increasing velocity ratio, the drag force applied on the particles by the gas will be smaller with increasing velocity ratio. The smaller the drag force will cause less reduction on the radial mean particle velocity. Second, the particle residence time decreases with an increase in the velocity ratio. Since the drag force which is responsible for the particle radial motion is a function of the radial mean velocity difference between the particle and gas, the decrease in the particle residence time will reduce the total time used to integrate the equation of motion. And this will cause less reduction in the radial mean particle velocity with an increase in the velocity ratio.

Radial Particle Dispersion

The higher radial particle velocity does not always indicate a higher particle dispersion. One way to measure the radial dispersion is to measure the directional angle of the particle velocity vector, $\alpha = \tan^{-1}(V_p/U_p)$. Figure 8 displays the radial profile of α for all

velocity ratios at x/di of 3 and 10. The plots show that at x/di of 3 and of 10, the directional angles are the same for all velocity ratios. The reduction in the radial mean gas velocity occurs proportionally with the increase in the axial mean particle velocity for all velocity ratios. The result indicates that the particle dispersion is the same for all velocity ratios. This result is important because it will tell us that there is no change in the radial distribution of the particle number density for the flow condition and particle properties used in this research. Thus, one would not expect a change in the NOx emissions due to the particle spacing as shown by Masutani et al (2).

Figure 9 compares the directional angel of velocity vector between the gas and the particle at x/di = 3 and 10. For velocity ratio of 0, the directional angle for the gas is larger than the particles, indicating that the radial dispersion of gas is larger than the particles. This trend is verified by the calculation of a particle Stokes number larger than 10. This result also confirms the use of the half jet width and the gas centerline velocity as the length and velocity scales of the fluid in calculating particle Stokes number. For velocity ratios of 1 and 1.8, it seems that the radial dispersion of particle is higher than the gas. This is not caused by the ejection of particles by the large eddies structures because the particle Stokes number is larger than 10 for both velocity ratios. This behavior is contributed by the presence of the annular stream that prohibits the expansion of the central jet and by the initial radial velocity of the particles.

Gas Turbulence

Figure 10 displays the axial and radial fluctuating gas velocities, u_g' and v_g' at x/d_i of 3 and of 10 for the three velocity ratios. As the velocity ratio increases, the turbulent mixing in the outer and inner shear layers becomes more intense due to the increase in the gradient of the mean axial gas velocity. This is shown by the increase in the radial and axial fluctuating gas velocities. The presence of the inner shear layer is shown by a local maximum in the axial fluctuating gas velocity for the velocity ratio of 1.8 (Figure 8a). The absence of local maximum in the axial fluctuating gas velocity in the inner shear layer for the velocity ratio of 1 is due to the zero velocity jump between the annular and the central jets. This indicates that the case with velocity ratio of 1 behaves in a similar way to the velocity ratio of 1, but with the jet diameter equal to the annular diameter.

Particle Turbulence

It is desired to understand the mechanism for the generation of the particle turbulence when we want to use the two-fluid model. Figure 11 displays the axial and radial fluctuating particle velocities, u_p' and v_p' with the 5% error bars at x/d_i of 3 and of 10. It is interesting to note that the axial fluctuating particle velocity behaves differently from the radial fluctuating particle velocity for different velocity ratios.

At x/d_i of 10, the case with velocity ratio of 0 has the highest value of axial fluctuating particle velocity followed by the case with velocity ratio of 1.8 and 1, respectively. By

considering this trend and the particle St number, it is not expected that the gas turbulence plays a role in generating particle turbulence, rather that the particle turbulence is generated by the gradient of the axial mean particle velocity. As the gradient of the axial mean particle velocity increases, the axial fluctuating particle velocity also increases, similar to the gas turbulence. The dependency of the axial fluctuating particle velocity on the gradient of the axial mean particle velocity has been observed previously in particle-laden jet experiments (3) and mixing layer experiments (21, 32) have also explained the generation of particle turbulence by the gradient particle velocity using the fan spreading theory. The fan spreading theory states that particles arriving at one point in a downstream location originate from different points upstream and bring with them axial mean velocity information. The difference in the axial mean particle velocity at different radial positions will contribute to a higher value of the axial fluctuating particle velocity.

The profile of radial fluctuating particle velocity is different from that of the axial fluctuating particle velocity. At x/d_i of 10, the radial fluctuating particle velocity increases with an increase in the velocity ratio, similar to the gas turbulence. This behavior is not due to gas turbulence, but it is due to the generation by the gradient of the radial mean particle velocity (Figure 6). At x/d_i of 3, the radial fluctuating velocities are the same since the radial mean particle velocities are the same for all velocity ratios.

Anisotropic behavior is observed in the particle turbulence in which the axial fluctuating particle velocity is higher than the radial one. One source for this difference is due to the difference in the magnitudes variation between the axial mean particle velocity and the radial mean particle velocity.

Gas Reynolds Stress

The Reynolds stress $\overline{u_g' v_g'}$, of the gas-phase is the time-averaged rate of momentum transfer due to turbulence and is correlated to the turbulent production by multiplying it with the gradient of the axial mean velocity. The radial profiles of the normalized Reynolds stress at x/d_i of 3 and of 10 are displayed in Figures 12a and 12b. At x/di =3, the local maximum for velocity ratio of 1.8 shows the more intense of turbulent mixing than the velocity ratio of 1. The Reynolds stress in the outer shear layer increases with an increase in the velocity ratio. This indicates that the gas Reynolds stress is related to the gradient in the axial mean gas velocity. Moreover, the production of gas turbulence will follow the same pattern.

Particle Reynolds Stress

Figure 13 displays the radial profiles of the particle Reynolds stress, $\overline{u_p' v_p'}$, for all velocity ratios at x/d_i of 3 and 10. The shapes of the radial profiles are different for different velocity ratios. There is a change in the sign between the case with velocity ratio of 0 and the other cases and this is expected due to the change in the profile of the axial mean particle velocity. For a velocity ratio of 1.8, the gradient of the axial mean particle velocity changes from a negative (at

the nozzle exit) to a positive value in the periphery of the jet centerline. Besides the sign change, the trend of the magnitude for the particle Reynolds stress is similar to the axial particle fluctuating velocity, in which the velocity ratio of 1 has the lowest magnitude. This result indicates that there is a strong relationship between the particle Reynolds stress and the gradient of the axial mean particle velocity. This information will be useful to close the particle Reynolds stress in the two-fluid model.

Hot-Flow Studies-University of Arizona

The furnace and annular burner have been constructed. Preliminary shake down tests utilizing natural gas are commencing. 2M cooled thermocouple probes are being calibrated against existing probes used in by the Combustion Research Group.

References

1. Masutani, S. M., Azuhata, S., Miyadera, H., and Hishinuma, Y.," Pulverized Fuel Combustion in a Turbulent Round Jet Burner," *J. Propulsion*, 97-103, March-April (1988).
2. Hardalupas, Y., Taylor, A.M.K.P., and Whitelaw, J.H.," Velocity and Particle-Flux Characteristics of Turbulent Particle-Laden Jets," *Proc. R. Soc. Lond*. A., **426**, 31 (1989).

3. Prevost, F., Boree, J., Nuglisch, H.J., and Charnay, G.," Measurements of Fluid/Particle Correlated Motion in the Far Field of an Axisymetric Jet," *Int. J. Multiphase Flow*, **22**, 4, 685 (1996).

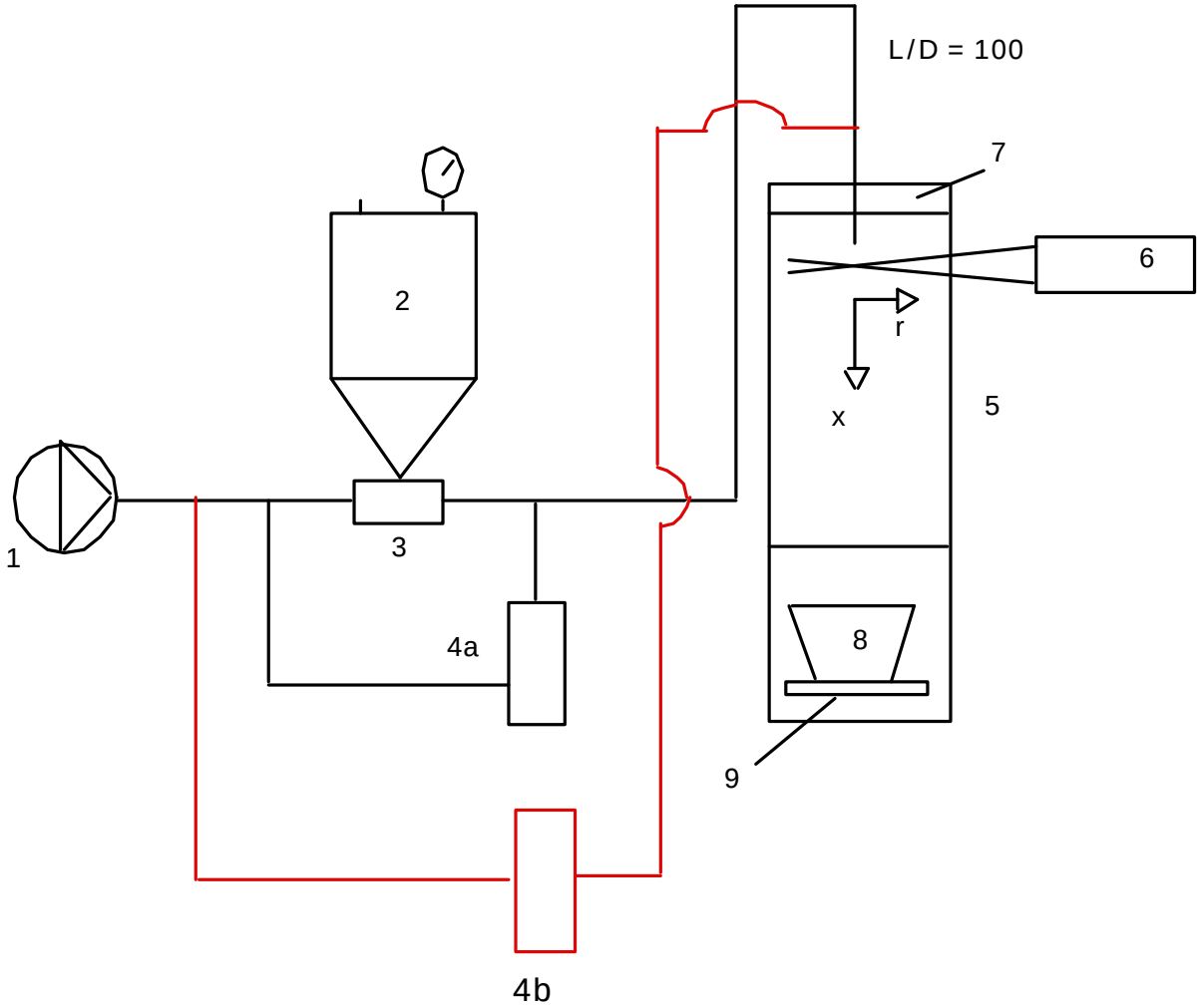

1. Compressed Air (80psi)
2. Particle Hopper
3. Inductor
4. Reverse Cyclone Seeder
    a. for central nozzle
    b. for annular nozzle
5. Test Chamber
6. LDV/PDPA
7. Honeycomb Flow Straightener
8. Particle Collection
9. Load Cell

Figure 1 Schematic Diagram of the Cold-Flow Experimental Setup

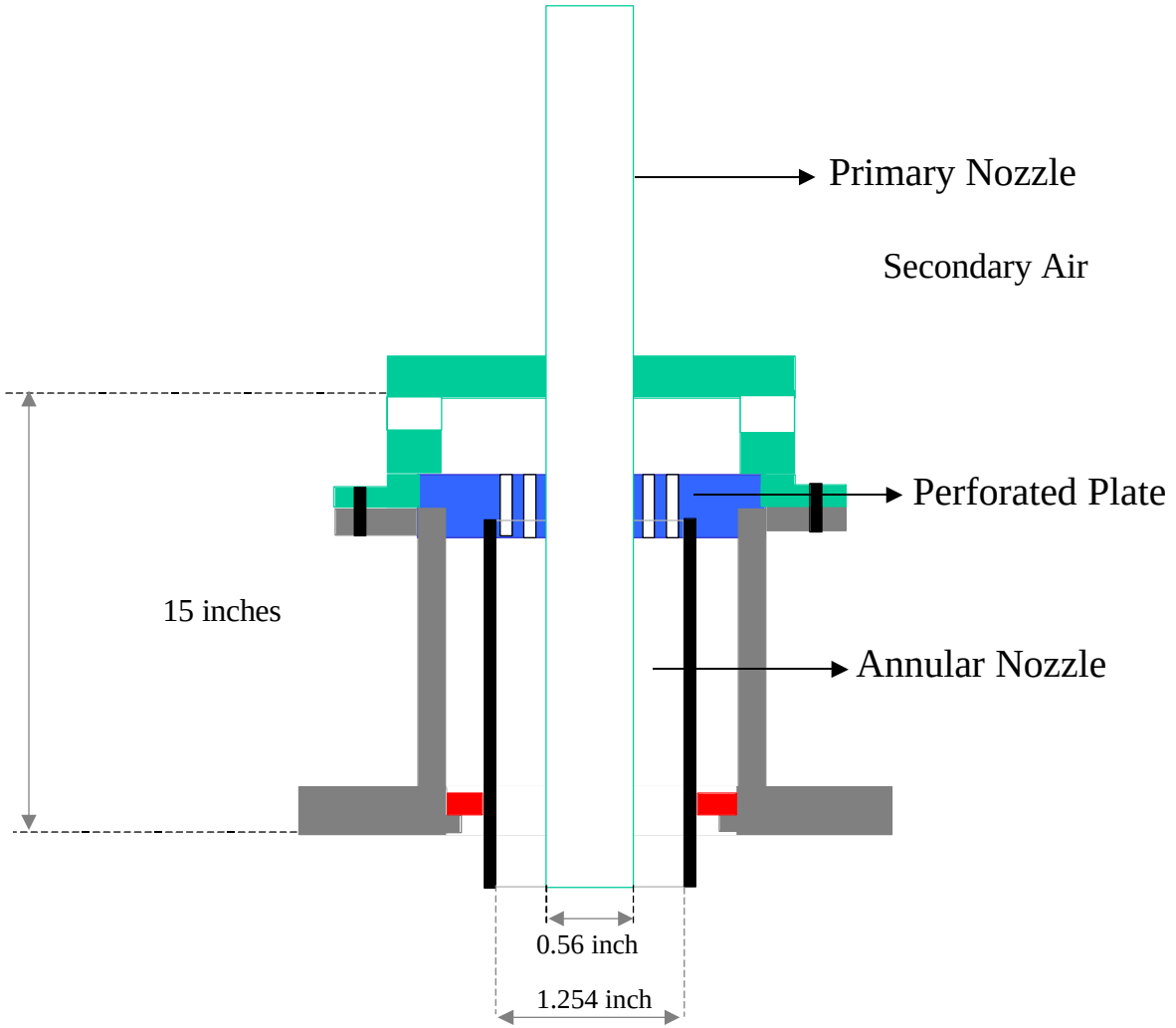

Figure 2 Detailed Schematic of Cold-Flow Primary and Annular Nozzles

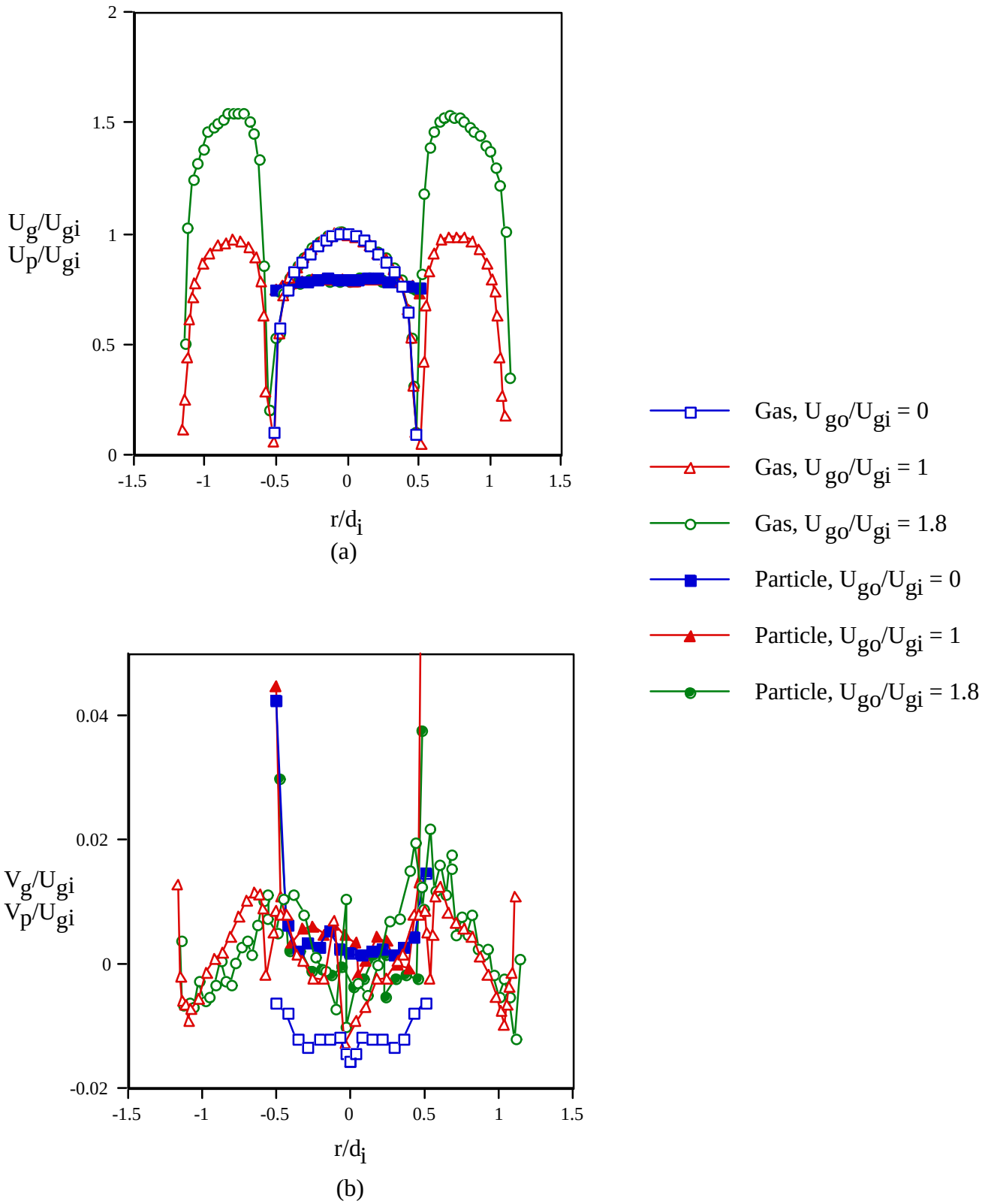

Figure 3 Gas and particle velocities at the nozzle exit (a) axial mean velocity, (b) radial mean velocity, (c) axial fluctuating velocity, and (d) radial fluctuating velocity

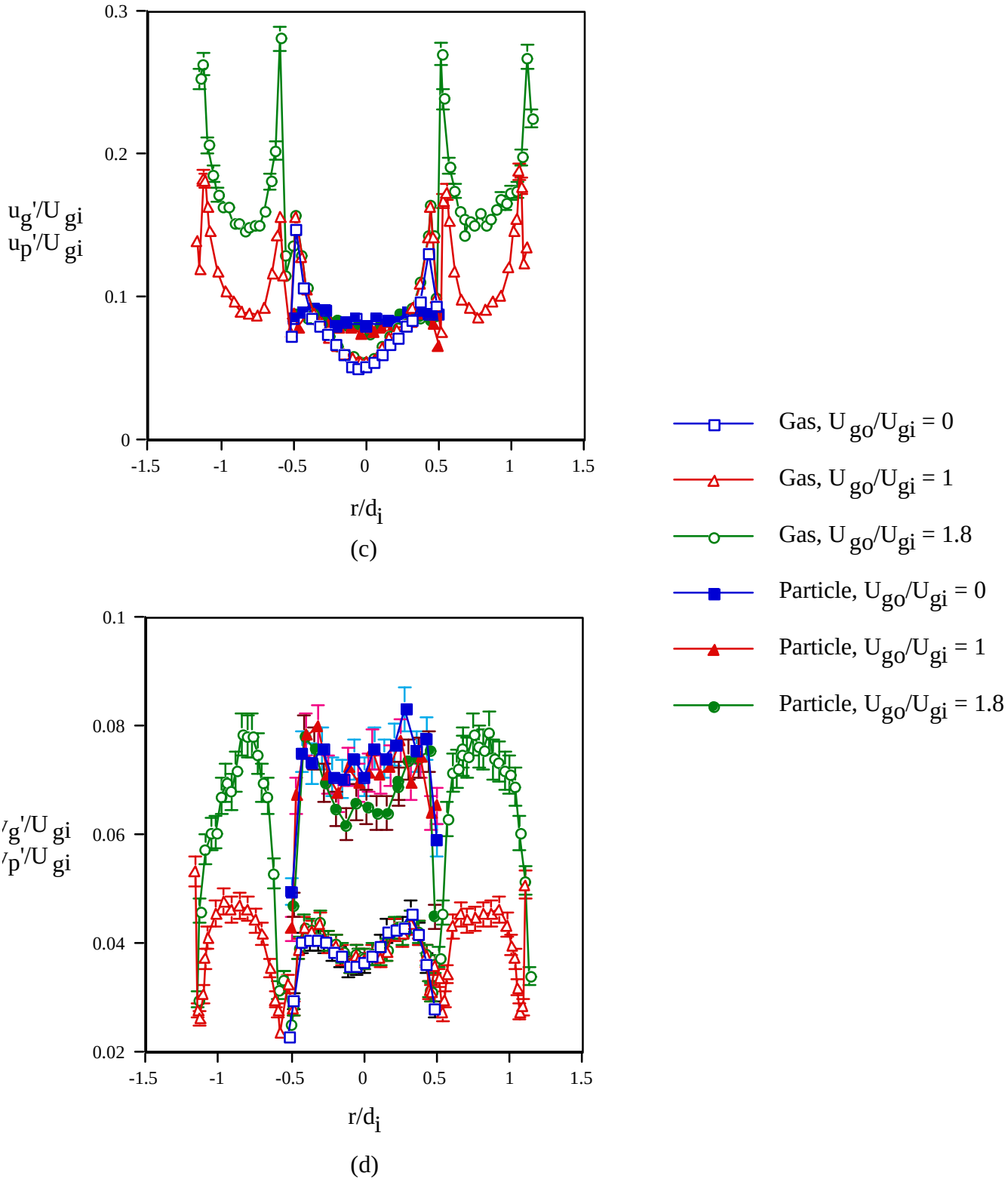

Figure 4. Gas and particle velocities at the nozzle exit (c) axial fluctuating velocity, and (d) radial fluctuating velocity

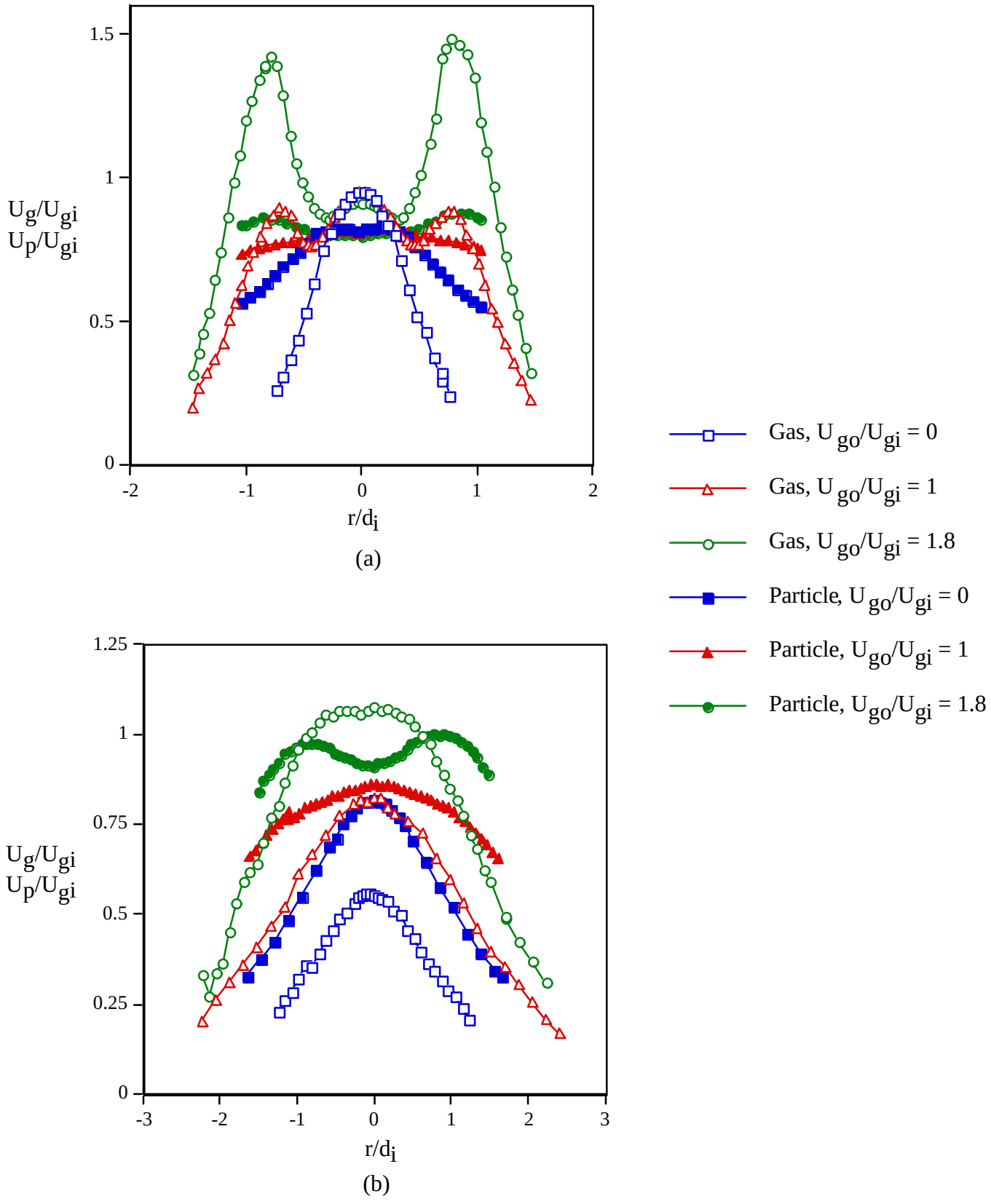

Figure 4. Axial mean gas and particle velocities at (a) x/di = 3 and (b) x/di = 10

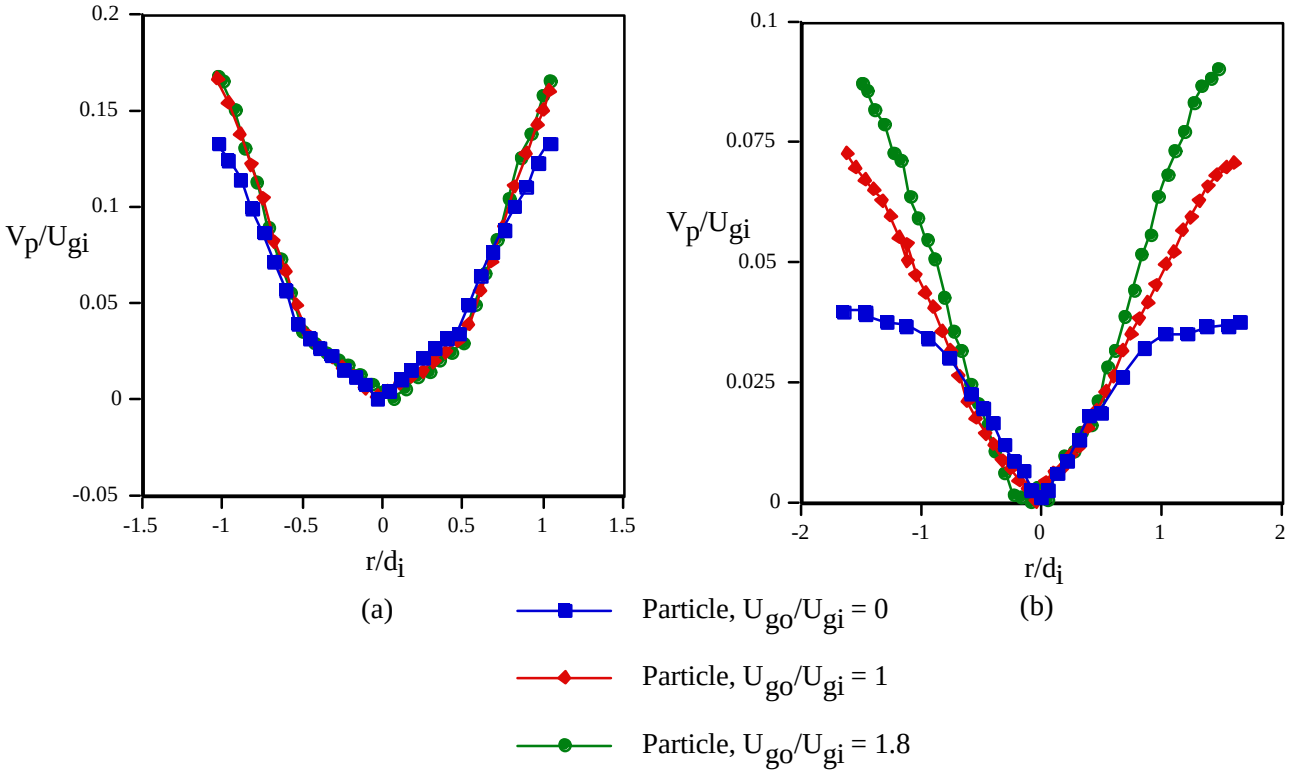

Figure 5. Radial particle velocity at (a) x/di = 3 and (b) x/di = 10

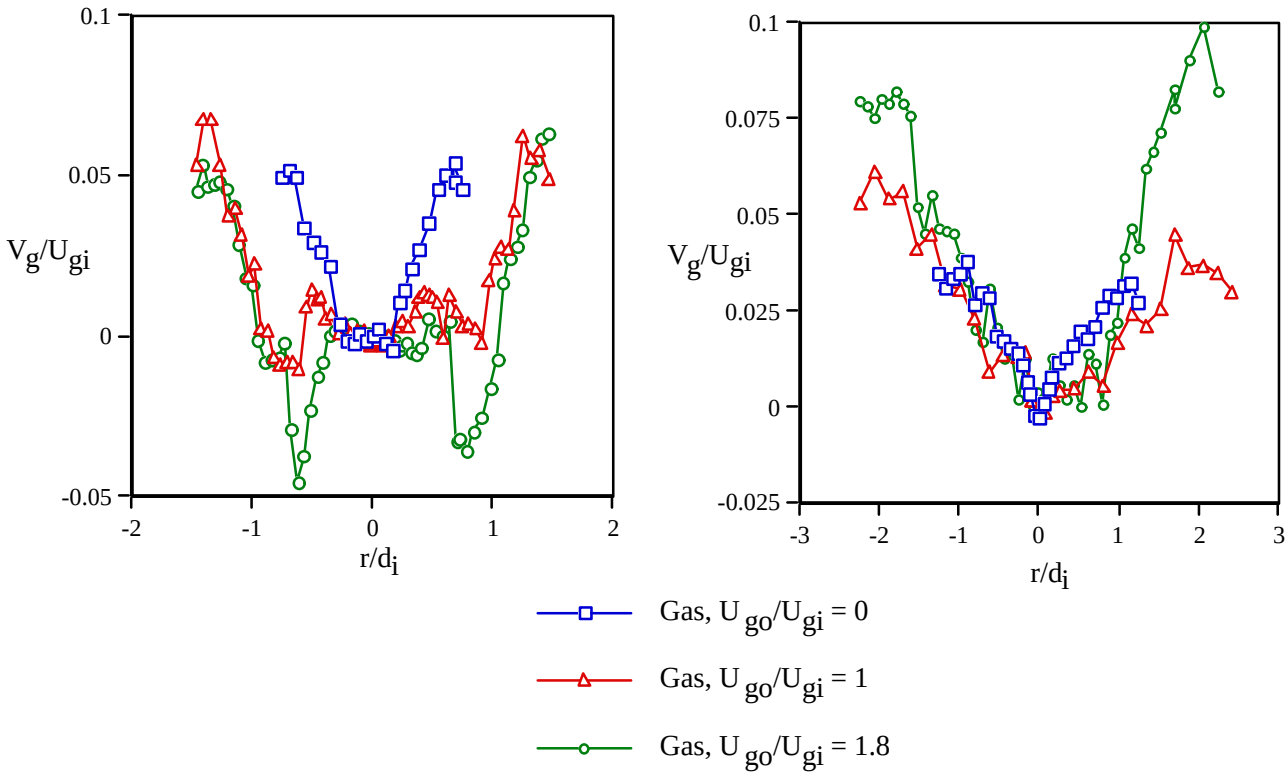

Figure 6. Radial mean gas velocities at (a) x/di = 3 and (b) x/di = 10

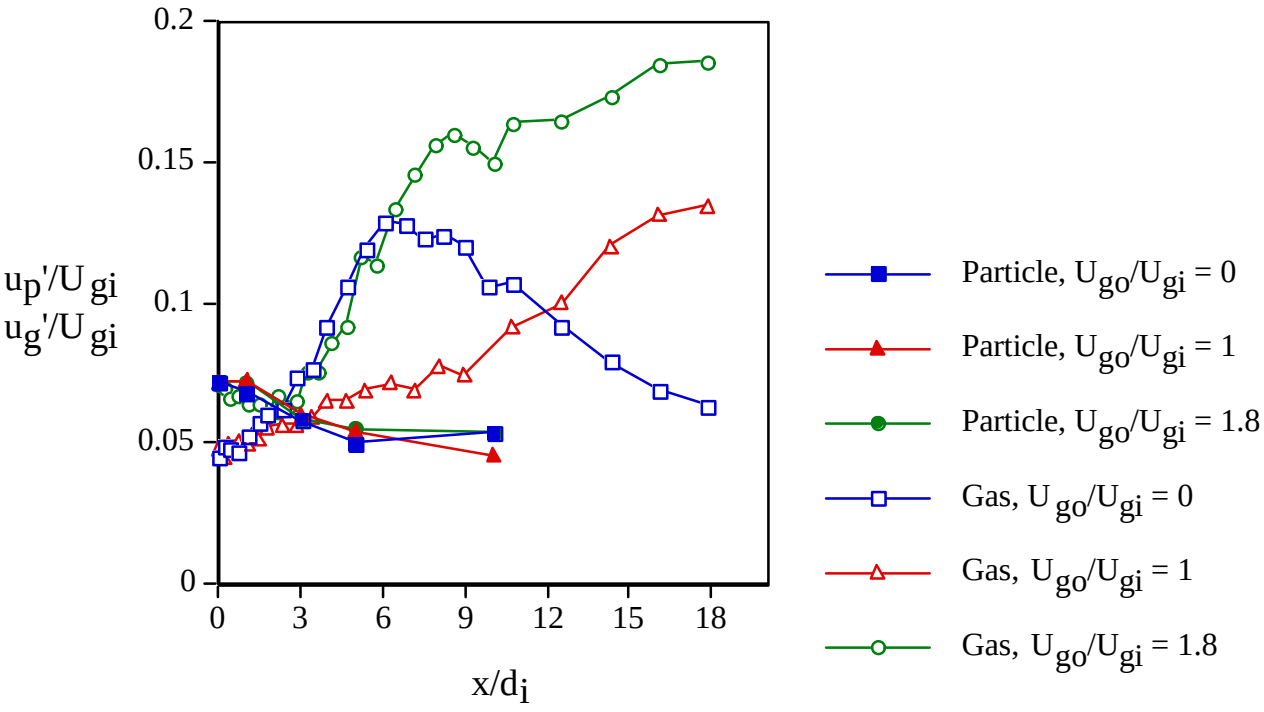

Figure 7. Axial evolution of the axial fluctuating gas and particle velocities along jet centerline

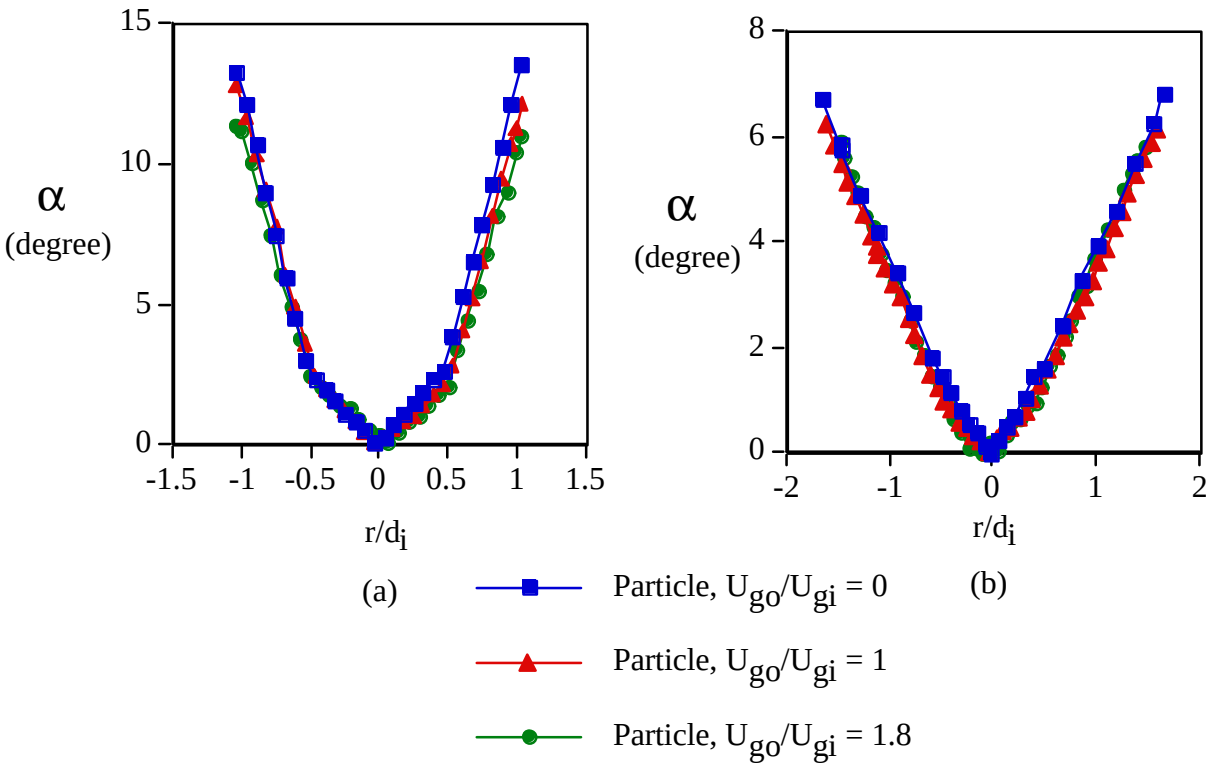

Figure 8. Directional angle, α of particle velocity vector at (a) x/d_i =3 and(b) x/d_i =10

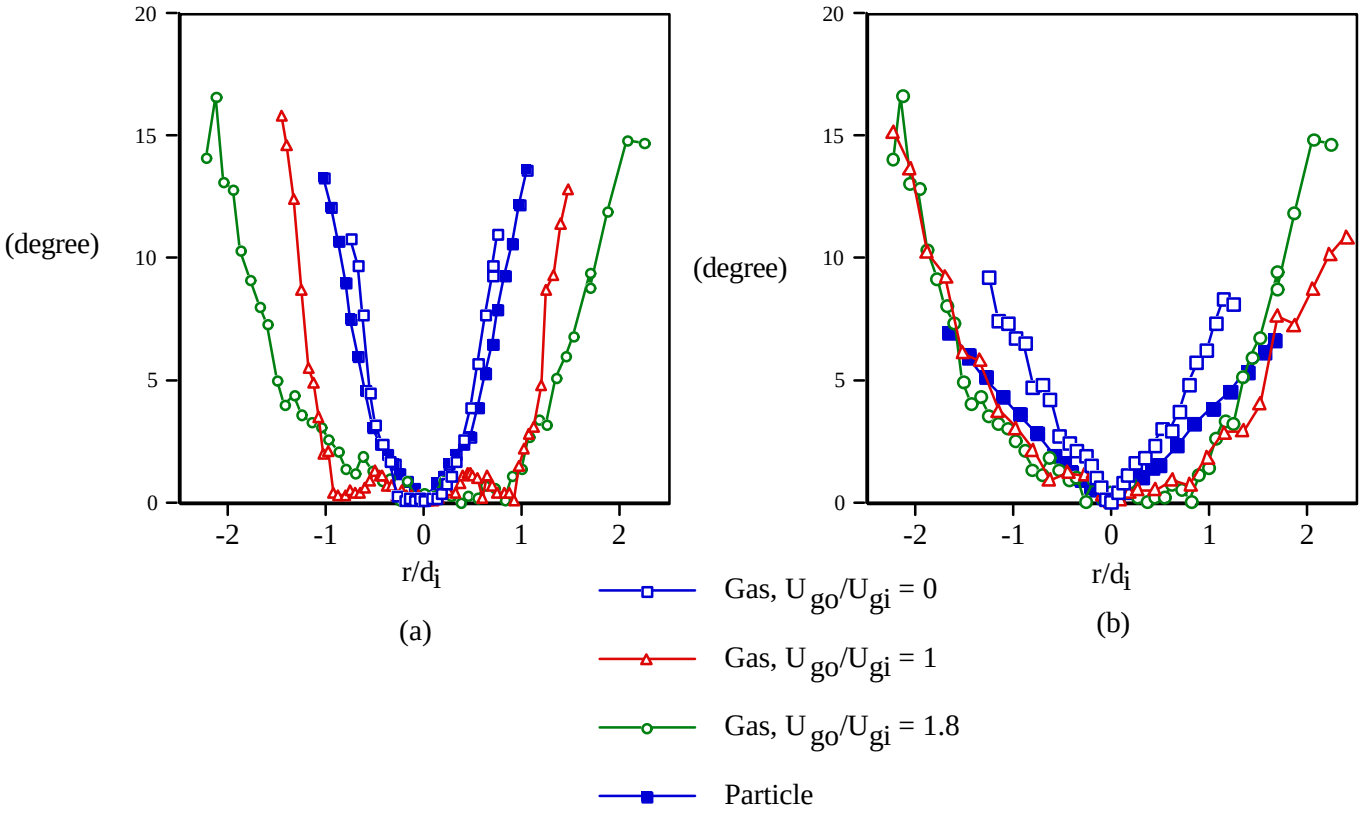

Figure 9. Comparison between the directional angle, α of velocity vector of the gas and particle at (a) x/di =3 and (b) x/di = 10.

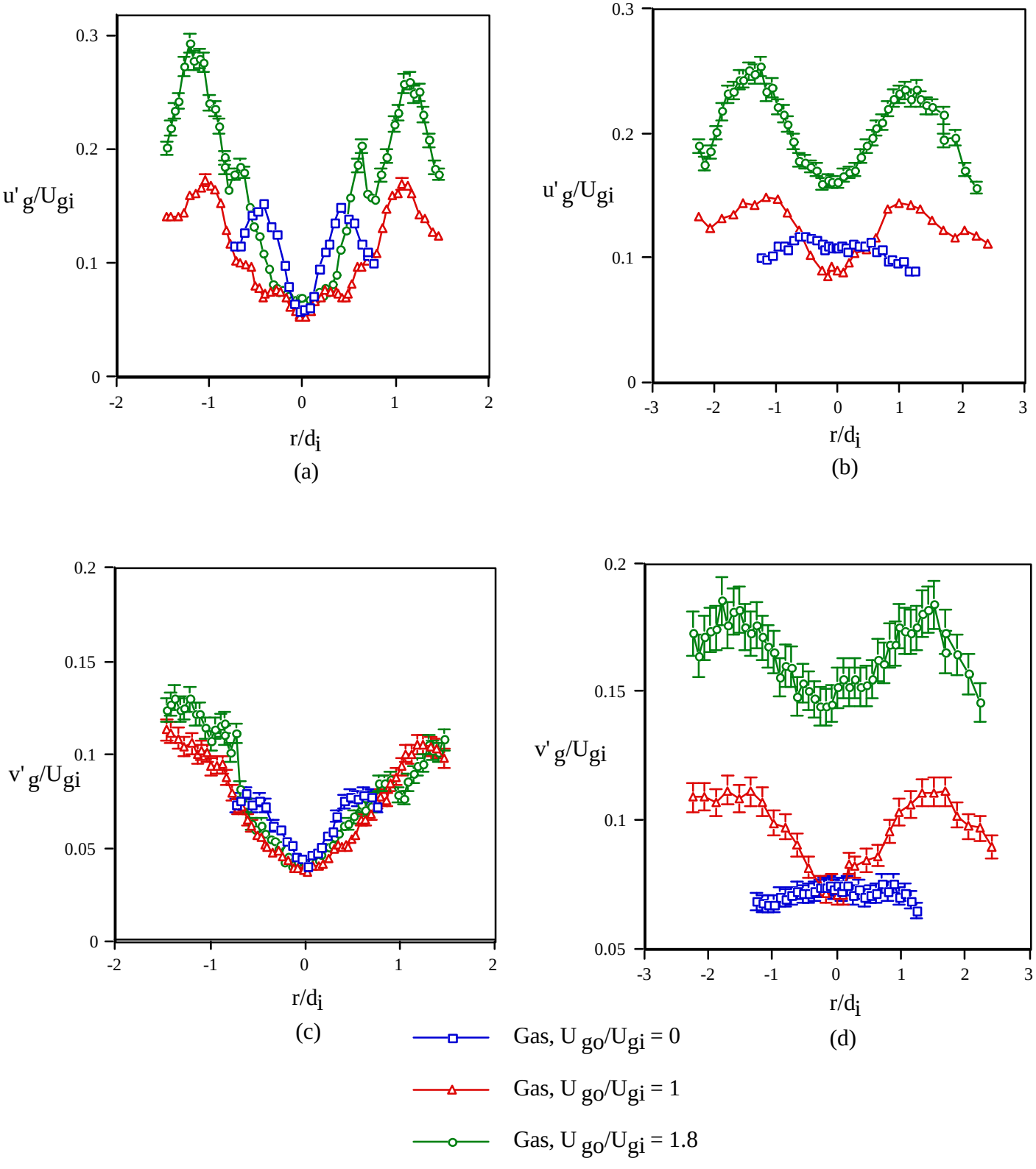

Figure 10. Axial fluctuating gas velocity at (a) x/di = 3 and (b) x/di = 10, and the radial fluctuating gas velocity at (c) x/di = 3 and (c) x/di = 10

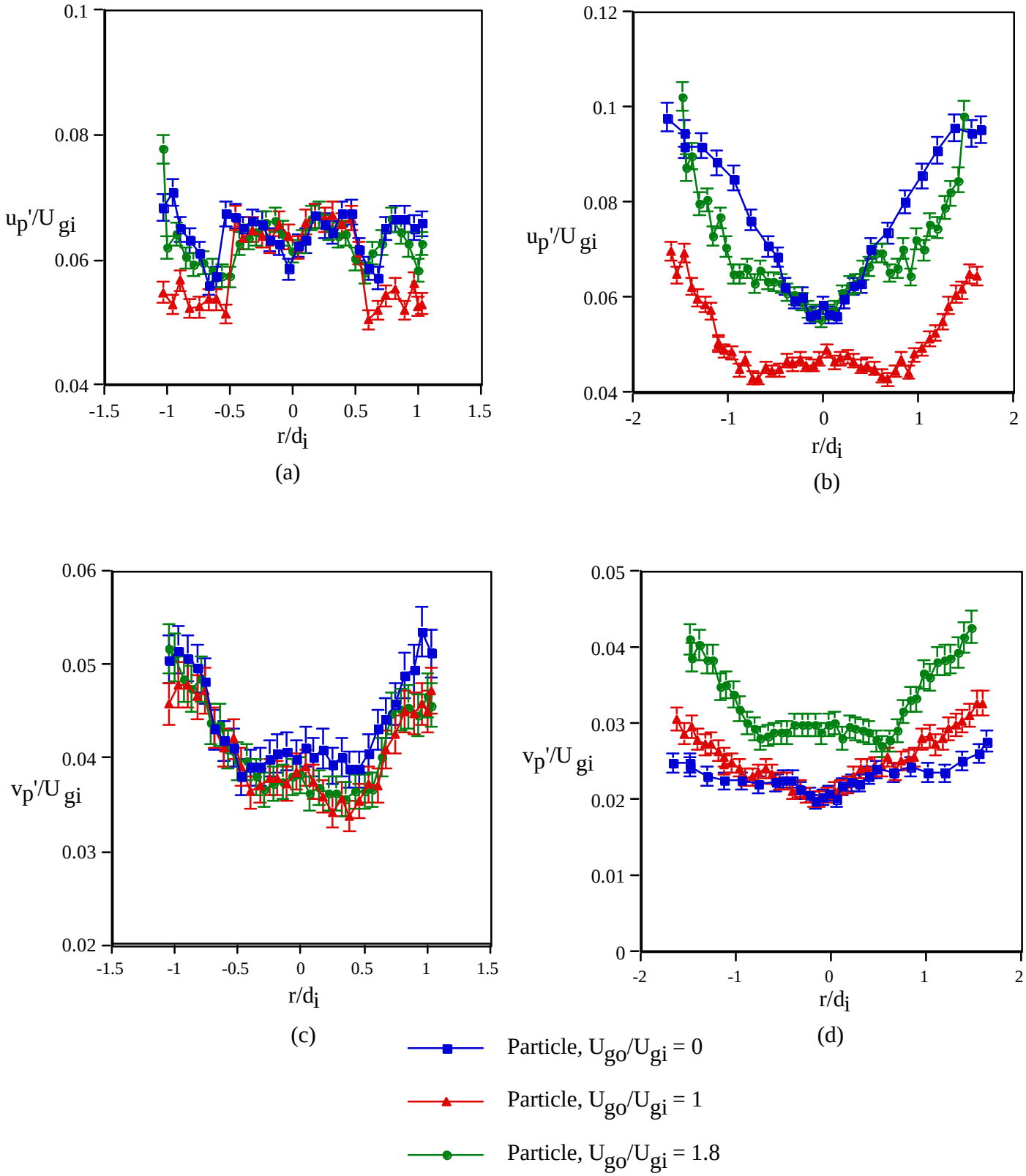

Figure 11. Axial fluctuating particle velocity at (a) x/di = 3, (b) x/di = 10, and the radial fluctuating particle velocity at (c) x/di = 3, (d) x/di = 10

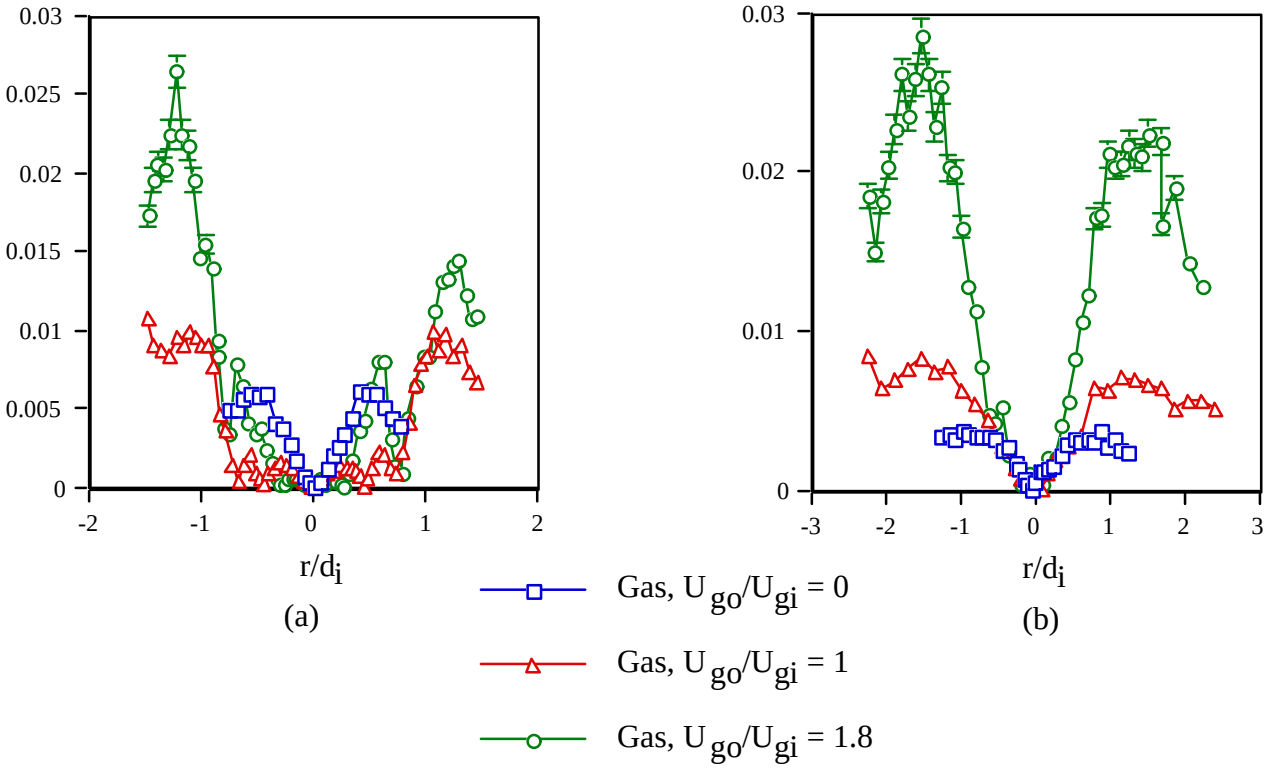

Figure 12. Reynolds stress of the gas-phase at (a) x/di = 3, (b) x/di = 10

Figure 13. Particle Reynolds stress at (a) x/di = 3, and (b) x/di = 10